

# Laterally Tunable Plasmon Resonance in Confined Biatomic-Layer Ag Nanodisks

Huajun Qin, Yi Gao, Jing Teng, Hongxing Xu, and Kehui Wu\*

Institute of Physics, Chinese Academy of Sciences, Beijing 100190, China

Shiwu Gao

Department of Physics, University of Gothenburg, SE-41296, Gothenburg, Sweden

**ABSTRACT** We report on the fabrication and investigation of the plasmon excitations in laterally confined quasi-two-dimensional (2D) Ag nanodisks on a Si(111) substrate. Different from the Mie resonance in Ag clusters and the propagating plasmon waves in 2D systems, these ultrathin nanodisks exhibit a low-energy plasmon resonance whose frequency is continuously tunable by the disk diameter. Quantum-mechanical simulations revealed the origin and the effects of screening and charge transfer on the plasmon excitation. The character and size-dependence are promising for engineering plasmonic and optical properties in supported 2D systems.

**KEYWORDS** Surface plasmon, Ag nanodisks, lateral confinement, atomic layer structures, electron energy loss spectroscopy

Plasmon excitation in nanostructures has been the focus of intensive research efforts during the past decade.<sup>1,2</sup> Unlike the bulk and surface plasmons, nanostructures sustain localized surface plasmon resonances (LSPR), whose frequencies can be controlled by their geometric parameters. An example is metallic nanoparticles and nanoshells, whose plasmon resonance frequency can be varied from the visible to the near-infrared regime.<sup>3–5</sup> The tunable frequency of LSPR has spurred tremendous interests for fundamental studies and offers promising applications in sensing, spectroscopy, photochemistry, and solar energy conversion. So far, both the number of tunable LSPR systems and the range of tunable frequencies are, however, still rather limited. For instance, the dipole plasmon frequency of spherical particles is only tunable between  $\omega_p/\sqrt{3}$  and  $\omega_p/\sqrt{2}$ ,<sup>6</sup> and nearly fixed at  $\omega_p/\sqrt{3}$  when the particles are small. Here  $\omega_p$  is the plasmon frequency of bulk solids. Similar limitation also applies for other types of nanosystems that are available.

On the other hand, low-dimensional systems, such as metal thin films with finite thickness and surface-states, support a low-energy acoustic plasmon mode, with a continuous spectrum between 0 and  $\omega_p/\sqrt{2}$ .<sup>7–9</sup> This mode corresponds to a propagating plasmon wave along the surfaces. It is particularly interesting as its low energy matches with various dynamic processes such as phonon excitation and Cooper pair formation. Unfortunately, this plasmon mode cannot be directly coupled with light due to the mismatch in energy dispersion. Moreover, the fact that the plasmon frequencies are dependent on the parallel

momentum  $q_{\parallel}$  could be another obstacle to select certain plasmon resonant frequency when  $q_{\parallel}$  are not matched. It is thus interesting and tempting to find out whether it is possible to fabricate quasi-two-dimensional (2D) structures that can possibly confine the low-energy plasmon wave into tunable resonance state, which can be utilized for novel optical applications.

In this letter, we report on the fabrication and observation of a new type of LSPR in a quasi 2D system: bilayer Ag nanodisks on a Si(111) substrate. These disks have identical height of two atomic monolayers (ML), and their radii are variable from about 7 to 20 nm. We observed a new low-energy plasmon mode below 1 eV, whose energy depends on the diameters of these disks. Theoretical simulations based on the linear response theory produced the size-dependence of this low-energy resonance. It also revealed the dipole character and the effects of substrate screening and charge transfer on the plasmon excitations in such supported 2D systems.

The experiments were carried out in an ultrahigh vacuum system (base pressure  $5 \times 10^{-11}$  mbar) equipped with a scanning tunneling microscopy (STM), low-energy electron diffraction (LEED), and high-resolution electron energy loss spectroscopy (HREELS, LK-5000). The Si(111) substrates were cut from a phosphorus-doped Si wafer with a resistivity of 2  $\Omega$ cm. Clean Si(111)  $7 \times 7$  surfaces were obtained by standard flashing to 1500 K. To grow Ag disks, a Si(111)  $\sqrt{3} \times \sqrt{3}$ -Ga surface was first prepared by evaporating one-third ML Ga atoms to a clean  $7 \times 7$  surface, followed by annealing at 800 K for 2 min. Ag was then deposited on the  $\sqrt{3} \times \sqrt{3}$ -Ga substrate at room temperature (RT), followed by slight annealing at 370 K for a few minutes. Each sample (with different Ag coverage) was grown at one deposition step to

\* To whom correspondence should be addressed. E-mail: khwu@aphy.iphy.ac.cn.

Received for review: 4/7/2010

Published on Web: 07/08/2010



avoid contamination during sample transfer. The as-prepared samples were transferred to the analysis chamber for in situ STM and HREELS investigations. The HREEL spectra were recorded with the incident angle of  $55^\circ$  with respect to the surface normal. The energy dispersion was measured by rotating the analyzer. The parallel wavevector of the surface plasmon ( $q_{||}$ ) was calculated from the energies and angles of incident and scattered electrons by  $q_{||} = [(2mE_i)^{1/2}/\hbar][\sin \theta_i - (1 - E_{\text{loss}}/E_i)^{1/2} \sin \theta_s]$ ,<sup>10</sup> where  $E_i$  is the incident beam energy, and  $\theta_i$  and  $\theta_s$  are incident and scattering angles. In our measurement, the momentum resolution was estimated to be about  $0.02 \text{ \AA}^{-1}$  at the incident beam energy of 20 eV.

The first step in our study is to prepare well-defined, quasi 2D Ag disks with a uniform and controllable size. It is worth to note that the growth of Ag on various substrates including the Si(111)  $7 \times 7$  has been studied extensively in the past.<sup>11–14</sup> However, the size, shape, and height of Ag islands are normally nonuniform. Besides, in the cases of semiconductor substrates, disordered wetting layers are usually formed in the initial stage, resulting in disordered, poorly defined interfaces. In this study, a Si(111)  $\sqrt{3} \times \sqrt{3}$ -Ga structure was introduced prior to the growth of Ag on Si. On this particular substrate, the growth of Ag becomes dramatically different. Figure 1 shows typical STM images as a function of the Ag coverage. Ag disks are found to distribute uniformly on the surface, and all disks exhibit an identical height of 4.6 Å, corresponding to two atomic layers of Ag(111). The (111) orientation of these islands was also confirmed by LEED where Ag(111) spots are identified (Figure 1g). These disks have a roughly round shape, and their sizes are quite uniform as seen from the statistical size distribution shown in the bottom of Figure 1. Moreover, between the Ag islands we see the clean  $\sqrt{3} \times \sqrt{3}$ -Ga substrate, indicating that no wetting layer is formed. The absence of a wetting layer is important, since a wetting layer consisting of random Ag clusters will also generate plasmon signals to confuse the analysis. With increasing Ag coverage, the Ag disks grow laterally while their height remains constant, and eventually a completed 2 ML Ag film will form. Therefore, the averaged size of the disks in the range from about 7 to 20 nm can be well controlled by adjusting the Ag disk coverage from 10 to 54%.

The thus-prepared Ag disk system is ideal for investigating the size-dependent electronic excitations in a quasi-2D system. Angle-resolved HREEL spectra were recorded for as-prepared samples with the Ag disk coverage from 10 to 73%, as shown in Figure 2a. For comparison, the HREEL spectrum of the clean Si(111)  $\sqrt{3} \times \sqrt{3}$ -Ga substrate was also shown. The spectrum of the clean substrate shows a semiconducting gap of about 0.8 eV and a broad feature above 1 eV arising from interband transitions, which is consistent with literatures.<sup>15,16</sup> In contrast, on surfaces with Ag disks, a remarkable new peak appears around 0.4 eV. Moreover, as the size of Ag disks increases, the peak energy

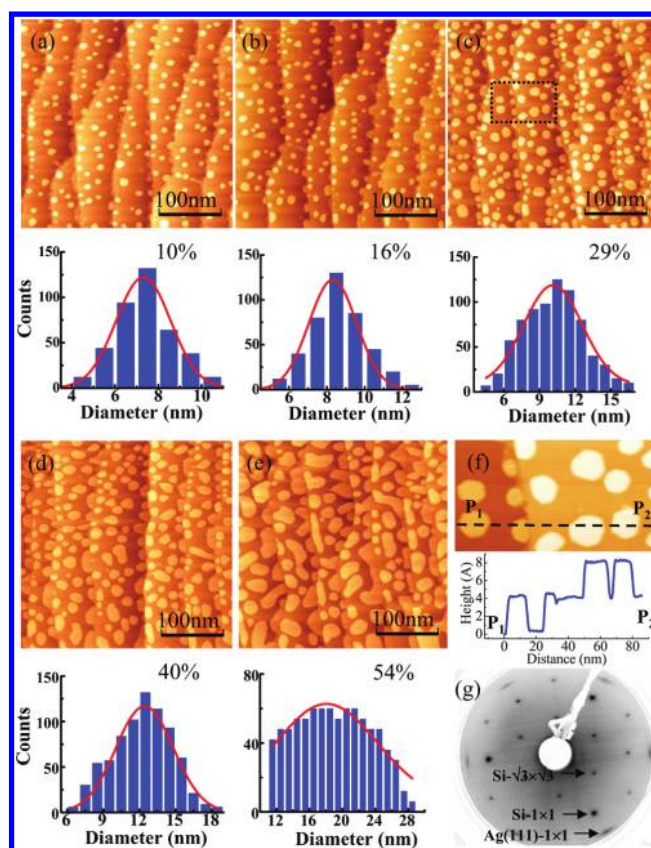


FIGURE 1. (a–e) The typical STM images of Ag disks grown on Si(111)- $\sqrt{3} \times \sqrt{3}$ -Ga at different Ag coverages. All Ag disks have an identical height of 4.6 Å. Beneath the STM images are plots showing the statistical distribution of the size of Ag disks as derived from STM images, and the curves are Gaussian fits. (f) The zoom-in image taken from the marked rectangle area in (c), and a line profile indicated by P1–P2 is shown below. (g) The LEED pattern taken from (c) showing Ag(111)- $1 \times 1$  spots, indicating that the Ag disks are (111) oriented. Note that the Ag- $1 \times 1$  spots are elongated along the circular direction. This is because of the small misalignment between the Ag(111) islands and the Si(111) substrate lattice.

redshifts, approaching to the elastic peak when the Ag disks start to percolate. A clear redshift of the peak position, from  $\sim 0.4$  eV to  $\sim 0.2$  eV, corresponding to an increase of the averaged Ag disk size from about 7 to 20 nm can be revealed. Note that below 0.2 eV, the loss peak merges into the Drude tail of the elastic peak and a quantitative determination of the peak position becomes difficult. In addition, the intensity of the loss peak also increases as the size of Ag disks increases. On the other hand, the angle-resolved HREELS measurement shows that the energy versus momentum has almost no dispersion in this system, implying that this is a localized excitation mode. An example of the angle-resolved measurement is shown in Figure 2c.

To confirm that the redshift of the peak is indeed due to the size effect, we performed an additional experiment by annealing a surface with Ag disks. After prolonged annealing, more islands aggregate, resulting in a larger averaged island size. As the height of Ag disks still remains at 4.6 Å, the total area of the Ag islands keeps unchanged (see the insets of

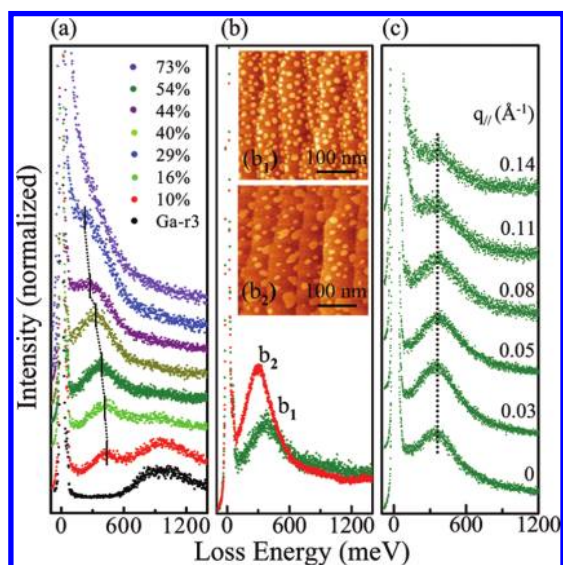


FIGURE 2. (a) The EEL spectra of samples with different Ag coverages, ranging from 10 to 73%. All spectra were taken at 90 eV incident beam energy, and normalized to the intensity of the elastic peak. (b) The EEL spectra of an as-prepared surface (b1) and the same surface after prolonged annealing (b2), respectively. The inset shows the morphology change of the surface due to the aggregation of Ag islands into larger islands. (c) The angle-resolved EEL spectra recorded on the surface with Ag coverage of 29%, showing that there is almost no change of the plasmon peak energy. These spectra were taken at 20 eV incident beam energy.

Figure 2b). The HREEL spectra obtained from the surface before and after annealing were shown in Figure 2b for comparison, and a red shift is clearly revealed.

To understand the origin of this excitation mode, we notice first that this mode is absent on a clean Si(111)  $\sqrt{3} \times \sqrt{3}$ -Ga surface, so it can only be associated with the Ag disks. Because the energy of this mode is size dependent, it is unlikely to assign it to any vibrational excitation, or interband transitions, as both of them should be size-independent. Therefore, it is most likely that this peak is due to the collective electronic excitation in Ag nanodisks.

To further understand this mode, we calculated the excitation spectra for a confined 2D electron gas (C2DEG) based on the linear response theory and random phase approximation (RPA). The method was extended from a previous model of confined 1DEG<sup>17</sup> and was corroborated in a series of first-principles calculations.<sup>18,19</sup> Here, the ground-state wave functions were products of the radial wave functions, which were generated by solving the Schrödinger equation in a disk with diameter  $d$ , azimuthal function  $e^{i\phi}$ , and a Gaussian function in  $z$  that mimics the ground state of the vertical confinement. Information on the collective excitation was deduced from the induced electron density  $\delta n(x, \omega) = -f d^3 x' \chi(x, x', \omega) \varphi^{\text{ext}}(x', \omega)$ , under an external potential  $\varphi^{\text{ext}}(\rho, \phi) = \rho \cos \phi$ . Here  $\chi$  is the density response function of the interacting system. It was obtained from the noninteracting response function via Dyson equation,  $\chi(x, x'; \omega) = \chi_0(x, x'; \omega) + f d^3 x_1 d^3 x_2 \chi_0(x, x_1; \omega) K(x_1, x_2) \chi(x_2, x'; \omega)$ .<sup>20</sup> Here kernel  $K$

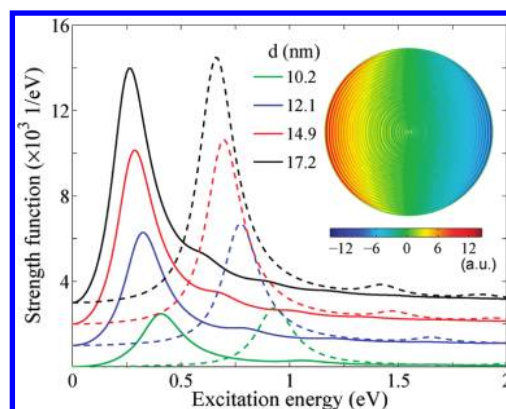


FIGURE 3. Calculated absorption strength function for Ag disks of different sizes. The dashed and solid lines indicate spectra of isolated Ag disks and of supported Ag disks where the substrate effects were included, respectively. The inset shows the calculated induced electron density oscillation for a supported Ag disk with diameter of 17.2 nm.

is the interaction between electrons, that is, the Coulomb interaction within RPA. The three-dimensional problem can be reduced to 1D by projection to symmetry-resolved angular functions and the Gaussian wave function in  $z$  as done in ref 17. The reduced 1D Dyson equation has then a symmetry resolved kernel

$$K_m(\rho_1, \rho_2) = (2\pi)^2 \sum_l \frac{(l-m)!}{(l+m)!} \frac{\tilde{p}_<^l}{\tilde{p}_>^{l+1}} [P_l^m(0)] / \epsilon \quad (1)$$

Here  $P_l^m(0)$  is the associate Legendre polynomial of quantum  $(l, m)$ ,  $\epsilon$  is a dielectric constant, and

$$\tilde{p}_<^> = \frac{1}{2} \left[ \sqrt{(\rho_1 + \rho_2)^2 + D^2/8} \pm \sqrt{(\rho_1 - \rho_2)^2 + D^2/8} \right] \quad (2)$$

which were defined by the vertical projection. In eq 2,  $D$  is the thickness of the Ag disk. The reduced 1D response function was solved similarly as in ref 17.

Figure 3 shows the simulated dipole strength functions for a number of disk diameter  $d$ . The dashed and solid curves correspond to spectra for the free-standing Ag disks and those adsorbed on the Si substrate, respectively. Here the  $d$  electrons of silver were included via an effective dielectric function  $\epsilon_d = 4$  and the effect of the substrate was also treated similarly by an additional dielectric constant  $\epsilon_{\text{Si}} = 15$ .<sup>20,21</sup> Both set of spectra are dominated by a main absorption peak located below 1 eV. As  $d$  increases, the energy of this peak gradually redshifts while its intensity grows almost linearly with the number of electrons in the disks. The diameter dependence of the plasmon energies are plotted in Figure 4, together with those extracted from EELS

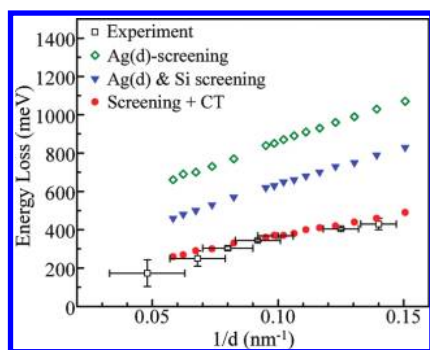


FIGURE 4. Energy dispersion versus the inverse of the disk diameter extracted from the peak positions in EEL spectra in Figure 2a (shown in open squares). Note that below  $0.05 \text{ nm}^{-1}$ , the loss peak merges into the Drude tail of the elastic peak and thus precise determination of the peak position becomes difficult. Theoretical simulations were performed for both free-standing (diamonds) and adsorbed Ag disks, taking into account substrate screening (triangles) and charge transfer effects (dots), respectively.

measurement. The two set of calculations show similar energy dispersions as a function of disk size and are in good agreement with the experimental data, although the simulated plasmon energies for the free-standing disks are higher than the experimental ones. Better agreement with experiment can be reached by further taking into account the charge transfer from the disks to the substrate. Indeed, our core-level X-ray photoemission spectra from the as-prepared samples showed a blue shift of the Ag  $3d_{5/2}$  peak, indicating a charge transfer from Ag to the substrate. This charge transfer should reduce the free electron density of the silver disks. To mimic this effect, we did calculations with a modified electron density  $r_s = 3.50$  (rather than  $r_s = 3.02$  usually used for the Ag, where  $r_s$  is the mean radius per free electron, in units of the Bohr radius). It amounts to a charge transfer of 0.3 electron per adatom. The calculated dispersion with substrate screening and charge transfer could then quantitatively reproduce the experimental data as shown in Figure 4. Although the effects of substrate screening and charge transfer were treated in a phenomenological manner in our simulation, our calculations capture the essential physics of these effects and should be reliable on the quantitative level.

In the inset of Figure 3, the distribution of the induced electron density is plotted for the plasmon mode in a Ag disk with  $d = 17.2 \text{ nm}$ . Apart from the Friedel oscillations across the whole disk, the dipole character of the collective oscillations is clearly visible. Comparing the data and simulation, we can conclude that the low-energy mode observed by experiment is indeed the dipole plasmon resonance of the

nanodisks, which is formed by the lateral confinement of the quasi-2D electron gas.

In conclusion, we found a tunable collective excitation mode in laterally confined, quasi-2D Ag disks prepared on Si. The energy of this collective excitation mode can be tuned continuously down to zero by controlling the size of the Ag disks, which is dramatically different from the conventional Mie resonance in nanoparticles. Combined with theoretical simulations, we have explained the origin and the excitation character of this mode. Interestingly, the low-energy of this plasmon mode, 0–0.4 eV, overlaps with the energies of typical molecular vibrations and surface phonon bands. Therefore our results have implications in controlling various plasmon-assisted processes at surfaces and nanostructured systems.

**Acknowledgment.** We thank Professor Peter Nordlander for his valuable discussions. This work was supported by the National Science Foundation (10874210), CAS, and MOST (No. 2007CB936800) of China, and STINT (Institutional grant), SSF (Metamaterial frame project) of Sweden.

#### REFERENCES AND NOTES

- (1) Barnes, W. L.; Dereux, A.; Ebbesen, T. W. *Nature* **2003**, *424*, 824.
- (2) Maier, S. A.; Kik, P. G.; Atwater, H. A.; Meltzer, S.; Harel, E.; Koel, B. E.; Requicha, A. A. G. *Nat. Mater.* **2003**, *2*, 229.
- (3) Fofang, N. T.; Park, T. H.; Neumann, O.; Mirin, N. A.; Nordlander, P.; Halas, N. J. *Nano Lett.* **2008**, *8*, 3481.
- (4) Oldenburg, S.; Averitt, R. D.; Westcott, S.; Halas, N. J. *Chem. Phys. Lett.* **1998**, *288*, 243.
- (5) Prodan, E.; Nordlander, P.; Halas, N. J. *Nano Lett.* **2003**, *3*, 1411.
- (6) Pitarke, J. M.; Silkin, V. M.; Chulkov, E. V.; Echenique, P. M. *Rep. Prog. Phys.* **2007**, *70*, 1.
- (7) Stern, F. *Phys. Rev. Lett.* **1967**, *18*, 546.
- (8) Nagao, T.; Hildebrandt, T.; Henzler, M.; Hasegawa, S. *Phys. Rev. Lett.* **2001**, *86*, 5747–5750.
- (9) Diaconescu, B.; Pohl, K.; Vattuone, L.; Savio, L.; Hofmann, P.; Silkin, V. M.; Pitarke, J. M.; Chulkov, E. V.; Echenique, P. M.; Faras, D.; Rocca, M. *Nature* **2007**, *448*, 57.
- (10) Rocca, M. *Surf. Sci. Rep.* **1995**, *22*, 1.
- (11) Smith, A. R.; Chao, K. J.; Niu, Q.; Shih, C. K. *Science* **1996**, *273*, 226.
- (12) Thürmer, K.; Williams, E. D.; Reutt-Robey, J. E. *Phys. Rev. B* **2003**, *68*, 155423.
- (13) Yu, Y.; Jiang, Y.; Tang, Z.; Guo, Q. L.; Jia, J. F.; Xue, Q. K.; Wu, K. H.; Wang, E. G. *Phys. Rev. B* **2005**, *72*, 205405.
- (14) Politano, A.; Formoso, V.; Colavita, E.; Chiarello, G. *Phys. Rev. B* **2009**, *79*, 045426.
- (15) Nicholls, J. M.; Reihl, B.; Northrup, J. E. *Phys. Rev. B* **1987**, *35*, 4137.
- (16) Landrock, S.; Jiang, Y.; Wu, K. H.; Wang, E. G.; Urban, K.; Ebert, P. *Appl. Phys. Lett.* **2009**, *95*, No. 072107.
- (17) Gao, S.; Yuan, Z. *Phys. Rev. B* **2005**, *72*, 121406 (R).
- (18) Yan, J.; Yuan, Z.; Gao, S. *Phys. Rev. Lett.* **2007**, *98*, 216602.
- (19) Yan, J.; Gao, S. *Phys. Rev. B* **2008**, *78*, 235413.
- (20) Ehrenreich, H.; Philipp, H. R. *Phys. Rev.* **1962**, *128*, 1622.
- (21) Aspnes, D. E.; Studna, A. A. *Phys. Rev. B* **1983**, *27*, 985.
- (22) Ekardt, W.; Penzar, Z. *Phys. Rev. B* **1991**, *43*, 1322.